Title page

Title: ***In vivo* subcellular ultrastructures recognized with Hilbert-differential-contrast transmission electron microscopy**

Contributors:

1 Yasuko Kaneko

Department of Regulation-Biology, Faculty of Sciences, Saitama University, Saitama 338-8570, Japan Tel: 048-858-3411 Fax: 048-858-3698

E-mail: yakaneko@post.saitama-u.ac.jp

2 Radostin Danev

Okazaki Institute for Integrative Bioscience, National Institutes of Natural Sciences

3 Koji Nitta

Department of Regulation-Biology, Faculty of Sciences, Saitama University

Kuniaki Nagayama

Okazaki Institute for Integrative Bioscience, National Institutes of Natural Sciences, & Department of Physiological Sciences, the Graduate University for Advanced Studies

Corresponding contributor: Yasuko Kaneko

Running title: *In vivo* ultrastructures recognized with HDC-TEM

Key words: electron microscope, phase contrast, *in vivo* structures, cyanobacteria, thylakoid, rapid freezing .

Total number of pages: 12

Total number of figures: 2

Abstract

We describe the first application of a novel electron microscopic technique to visualize subcellular structures in a near-living state. Rapidly frozen ice-embedded cells provide the most realistic images, as they are free from artifacts induced by sample preparation such as chemical fixation, dehydration, staining and sectioning. The application of the conventional transmission electron microscope to ice-embedded cell imaging, however, has been limited by the low image contrast. The recently developed Hilbert-differential-contrast transmission electron microscope, which exhibits an unexpectedly high contrast, akin to the differential-interference-contrast in visible light microscopy, enabled us to clearly discern detailed subcellular structures in ice-embedded cyanobacterial cells.

Main text

Transmission electron microscope (TEM) images of biological samples without heavy element staining exhibit very weak contrast. To enhance contrast, two methods are typically employed: i) scattering contrast with small aperture diaphragms and ii) defocus contrast with deep defocusing [1]. The former technique is used in the histochemical sciences, where sectioned samples of cells or tissues are imaged, and the latter is popular in electron crystallography, where very thin samples are used. In both methods, however, the contrast is gained by impairing the intrinsically very high resolution of the TEM. This can be overcome through the use of phase contrast methods, techniques using phase plates, which are frequently applied in visible light microscopy (LM). Due to the fundamental issue of the electric charge imparted to phase plates by electron collisions [1], this has not yet been applied to TEM. We have carefully studied the phenomenon of electric charging [2,3] and

described several novel forms of electron-phase microscopy: Zernike-phase-contrast (ZPC)[4], Hilbert-differential-contrast (HDC) as mentioned [5,6], and complex observation [7].

Among these methods, HDC, of which the experimental schematics are shown in Fig. 1a, is particularly useful owing to its high contrast. Unlike differential-interference-contrast (DIC), HDC can be brought about only by inserting a phase plate to the back focal plane of the objective lens (Fig. 1a). The π-phase plate covering the half plane of the aperture converts the phase retardation by transparent objects to amplitude contrast. Image formation theory recognizes this conversion as the conversion of the image modulation function, the so-called contrast transfer function (CTF), from the sine functional modulation unique to conventional TEM (CTEM) (Fig. 1c) to the cosine functional one [1,5]. Due to the intense low frequency components recoverable with the cosine CTF, HDC can provide high contrast. Contrary to ZPC [4,7], which also carries the cosine CTF, the HDC CTF is an odd function characterized by a big jump at the frequency origin [5]. This odd nature is transferred to the point spread function (PSF) of HDC, which has an antisymmetric profile as shown in Fig. 1b. The antisymmetric double peak, which stands in contradistinction to the symmetry of the conventional PSF (Fig. 1d), is responsible for the differential contrast [5].

The phase retrieval for phase objects simply based on a spatial filter as shown here is not necessarily new. A differential kind of image contrast has already been reported with a lens system [8], where an optically processed Hilbert transform was first reported with a half plane π-phase plate. But due to the difference in the detection scheme, whether or not the primary wave background is utilized as origin of interference as described in Fig. 1a, what was actually observed, is the square of the differential image.

Ice-embedded whole cyanobacterial cells were observed by the HDC-TEM to assess the potential of the microscope for biological application, in particular the visualization of subcellular structures in a near-living state.

The experiments were carried out on a JEOL JEM-3100FFC electron microscope operated at 300 kV acceleration voltage with or without the HDC phase plate. The phase plates were prepared from amorphous carbon films. The films were deposited by vacuum evaporation (JEOL JEE-400) on a freshly cleaved mica surface. For observations at 300 kV acceleration voltage the film thickness corresponding to the π-phase plate was around 64 nm. At that thickness the transparency to 300 kV accelerated electrons was estimated to be 52% [4]. After preparation, the films were floated on a water surface and then transferred onto a molybdenum objective lens aperture with multiple holes with a diameter of 50 μm. Square holes of about 20 μm to maintain the cut-off frequency corresponding to a 2 nm spatial resolution, were cut asymmetrically using a focused ion beam machine (JEOL JFIB-2000)[4,5].

The microscope was equipped with an FEG electron gun and omega type energy filter. Objective lens parameters were: spherical aberration coefficient 5 mm, chromatic aberration coefficient 4.7 mm. All observations were performed with a nominal magnification of 10,000 and electron dose of about 100 e^-/nm^2 in zero loss filtering mode. The energy window width was set at 10 eV. A special aperture holder with heating was used to support the phase plates. To avoid contamination, the phase plates were kept at around 200°C at all times. All images were recorded with a Gatan MegaScan795 2K x 2K CCD camera [4,5]. Ditgital Micrograph, supported by Gatan, was used for image analysis.

The electron dose on the specimen could not be determined precisely, because of the scattering absorbance by the ice (more than 1μm thick) surrounding the specimen. The electron dose on the CCD, however, could be measured accurately as 10.5 e/nm^2 for CTEM and 8.1 e/nm^2 for the HDC-TEM method. The CCD dose by HDC-TEM was lower because of the scattering absorbance by the phase plate. Considering the position of the CCD camera,

final magnification was calculated as 16,000. Since physical pixel size of the CCD was 30 μm, the resolution was 1.78 nm/pixel, which gives a Nyquist wavelength of 3.56 nm (0.28 nm^{-1}).

Synechochoccus sp. PCC 7942 was cultivated on agar BG-11 medium under continuous light (60μE·$m^{-2}s^{-1}$) at 27±2ºC. The cells were collected in 0.2 M sucrose solution by centrifugation and dropped on a copper grid coated with carbon film. After removing excess liquid carefully with the tip of a filter paper, the sample was frozen rapidly in liquid ethane using a LEICA rapid freezing device (LEICA EM CPC). The grid with ice embedded cells was transferred to the specimen chamber of the TEM using a cryo-transfer system.

For conventional chemical fixation, the cells were fixed in 2% glutaraldehyde in 0.05 M potassium phosphate buffer (pH7.0) for 2 h at room temperature and in a refrigerator overnight. After rinsing in buffer, the cells were postfixed in 2% OsO_4 in buffer for 2 h at room temperature. They were then dehydrated in an acetone series and embedded in Spurr's resin. Ultrathin sections (silver-gold) were cut with a diamond knife on a Sorvall MT2-B ultramicrotome. After staining with uranyl acetate and lead citrate, the sections were observed with a Hitachi H-7500 TEM at an acceleration voltage of 100 kV with a nominal magnification of 10,000 and an electron dose of 300 e^-/nm^2.

Fig.1

The differential feature together with the high contrast is demonstrated in Fig. 1e for an ice-embedded whole cell. At first, one may mistake it for a conventional DIC image, but the high resolution attained with a 300kV TEM is two orders of magnitude better than that attainable with LM-DIC. Counterexamples obtained with CTEM are shown in Figs. 1f and g. An obscure, structureless image is observed in CTEM for the sample shown in Fig. 1f, which was taken under the same experimental conditions as for Fig. 1e except for the phase plate

and the defocus. The unexpectedly large difference in contrast between the two images (Figs. 1e and f) is likely attributable to the difference in the CTF coupled with the large defocus variation in the unusually thick whole cell sample. The cosine CTF characterizing HDC-TEM is less sensitive to the variation of defocus than the sine CTF once the just focus is set near the depth-center in the sample. The defocus needed to make the first zero of the cosine CTF coincide with the Nyquist frequency was calculated to be 3.2 μm.

Since no cyanobacterial structure was discerned by CTEM with a slight defocus close to the just focus used for the HDC-TEM (data not shown), the CTEM image was taken at a deep defocus of 15 μm to obtain an image with the best contrast as an illustration of what is attainable by CTEM, so as not to unfairly discredit the CTEM in the comparison.

Comparing another pair of images, the ice-embedded whole cell (Fig. 1e) and the plastic-embedded sectioned cell (Fig. 1g), we recognize a large difference in appearance which may be attributable to the enormous difference in specimen treatment. In the sectioned cell, first of all, we see a ragged cell wall, which reminds us that some shrinkage of the cell has occurred during preparation. Many aggregates and associated voids, which are indubitably induced by chemical treatment such as dehydration and selective staining of cellular organelles can also be recognized. On the other hand, the images of the ice-embedded cell are smoothly round and recognizably space-filled everywhere. Notice here that the rapid freezing is expected to preserve the overall structure, such as the cell shape, as well as subcellular structures. The preserved roundness of cyanobacterial cells allows us to estimate the specimen thickness to be about 1 μm.

Considering the deep focal depth of the 300 kV HDC-TEM, the image obtained should be a projection image of the 1μm thick specimen. We did not expect at the beginning that individual organelles, proteins and DNA could be visualized in the projection image of such a thick specimen, because the partial structures should overlap. However as we present here,

the ultrastructural details could be recognized in this condition. This fact in itself is a surprising discovery. There are two possible explanations for this unexpected result. First, cyanobacteria have relatively sparse structures and abundant water content. Second, in the case of the thylakoid, high contrast was gained because of its massive structure and overlapping of constituent lipid molecules in the direction of focal depth. Obviously none of these images could be brought about without HDC-TEM.

Fig. 2

Novel features of intact subcellular structures found in cyanobacterial cells are shown in Fig. 2. Close-up views of inner portions of cells and putative ultrastructural identifications are shown. The four examples provided were gathered from various cell images based on their structural similarities to CTEM images taken for plastic-embedded cells. Past reports using CTEM were referred to for the identification of thylakoid [9], Rubisco [10], polyribosome [11] and phycobilisome [12]. While the structural similarities and distribution within the cells were utilized for the identification, the procedure was not a simple pattern recognition. As is characteristic of DIC microscopy, HDC adds completely novel morphological features to TEM images. This has made the comparison between the conventional thin section image (Fig. 1g) and the ice-embedded one (Fig. 1e) an unconventional task. Even though restoring the normal contrast from the differential one by a mathematical procedure [13] may ease the task of image interpretation, the identification for the subcellular structures has to be confirmed by immuno-labelling or other methods.

Nevertheless, there are several ultrastructural features that can be more clearly recognized by HDC-TEM than by conventional methods. One can see numerous arrays of globular structures (circled in Fig. 2b) that are embedded in thylakoid membranes, possibly components of photosystems or other membrane proteins [9]. Some of these structures have an elongated shape and appear to be sticking out of the membrane. In the cisternal space of

the thylakoid membranes, bridge-like structures (arrows in Fig. 2b) are occasionally observed, which seem to connect two facing thylakoid membranes. Many polyhederal bodies (carboxysomes) can be easily recognized, and moreover, the packed constituent Rubisco molecules [10] (circled in Fig. 2c) can be distinguished. Polyribosomes (circled in Fig. 2d) often extend towards thylakoid membranes, where translation products may be needed. Phycobilisomes (circled in Fig. 2e) appear to be attached to thylakoid membranes through rod-like structures (arrows in Fig. 2e). These detailed ultrastructures revealed by HDC-TEM must be associated with specific functions, which have yet to be determined.

HDC-TEM with its extraordinary high contrast for unfixed, undehydrated and unstained biological samples may provide a novel kind of structural information useful in ultrastructural studies in microbiology, metabolic engineering and molecular biological monitoring in cell biology.

Acknowledgements

This research is partially supported by the Ministry of Education, Science, Sports and Culture, Grant-in-Aid for Creative Scientific Research, 2001-2006, 13GS0016. We are thankful to Messrs. H. Okawara and T. Itoh for making phase plates. We also thank Dr. H. Nakamoto for the cyanobacterial strain and helpful comments.

References

1 Reimer L (1997) *Transmission Electron Microscopy,* 4th ed. (Springer).

2 Danov K, Danev R, and Nagayama K (2001) Electric charging of thin films measured using the contrast transfer function. *Ultramicroscopy* **87**: 45-54.

3 Danov K, Danev R, and Nagayama K (2002) Reconstruction of the electric charge density in thin films from the contrast transfer function measurements. *Ultramicroscopy* **90**: 85-95.

4 Danev R, and Nagayama K (2001) Transmission electron microsocpy with Zernike phase plate. *Ultramicroscopy* **88**: 243-252.

5 Danev R, Okawara H, Usuda N, Kametani K, and Nagayama K (2002) A novel phase-contrast transmission electron microscopy producing high-contrast topographic images of weak objects. *J. Biol. Phys.* **28**: 627-635.

6 Nagayama K, and Danev R (2004) Differential contrast transmission electron microscope and method of processing data about electron microscope images. USA patent: US6,674,078 B2 (Jan. 6, 2004).

7 Danev R, and Nagayama K (2001) Complex observation in electron microscopy. II. Direct visualization of phases and amplitudes of exit wave functions. *J. Phys. Soc. Jpn*. **70**: 696-702.

8 Lowenthal, S. & Belvaux, Y. Observation of phase objects by optically processed Hilbert transform. Appl. Phys. Lett. **11,** 49-51 (1967).

9 Sherman D M, Troyan T A and Sherman L (1994) A Localization of membrane proteins in the cyanobacterium Synechococcus sp. PCC7942. *Plant Physiol*. **106**: 251-262.

10 Orús M I, Rodríguez M L, Martínez F and Marco E (1995) Biogenesis and ultrastructure of carboxysomes from wild type and mutants of Synechococcus sp. strain PCC7942. *Plant Physiol*. **107**:1159-1166.

11 Alberts B, Johnson A, Lewis J, Raff M, Roberts K, and Walter P (2002) *Molecular Biology of the Cell,* 4th ed. (Garland Science).

12 Fogg G E, Stewart W D P, Fay P and Walsby A E (1973) *The Blue-Green Algae*, (Academic Press).

13 Danev R and Nagayama K (2004) Complex observation in electron microscopy: IV. Reconstruction of complex object wave from conventional and half plane phase plate imaging pair. *J. Phys. Soc. Jpn*. **73**: 2718-2724.

Figure legends

Fig. 1 Schematics of two kinds of TEMs (**a**, **b**) and images taken with the two TEMs (**c**-**e**). (**a**) Schematics of Hilbert-differential-contrast (HDC)-TEM. The π-phase plate, set exactly at the back focal plane where usually an aperture is situated as in (**c**), functions to convert the original wave function of scattered electrons from Ψ to –Ψ Therefore the half-plane π-phase plate acts as a spatial filter of signum function in a selected dimension, leading finally to Hilbert transform in the real space [5,8]. The filtered wave function superposes on the background originating from the primary plane wave (1) on the image plane and yields an interference responsible for the HDC image. The crucial condition for the scheme to work is the existence of the strong background without the interception of the central beam by the π-phase plate. (b) Schematics of the point spread function, which is the Fourier transform of the odd cosine CTF characteristic of the HDC-TEM. A Gaussion envelope function was multiplied to the cosine CTF adjusted to an optimum focus [4]. (**c**) Schematics of conventional TEM (CTEM). There is no electron intercepting material at the aperture. The original wave function (Ψ) superposes on the background (1) and yields an interference responsible for the conventional image. (d) Schematics of the point spread function, which is the Fourier transform of the sine CTF of conventional TEM. A Gaussion envelope function was multiplied to the sine CTF adjusted to a Scherzer focus [1]. (**e**) 300 kV HDC-TEM image of an ice-embedded whole cell (near focus). (**f**) 300-kV CTEM image of the same ice-embedded whole cell as shown in (**a**) (~15μm defocus). (**g**) 100-kV CTEM image of a plastic-embedded, sectioned and stained cell.
Scale bars, 500 nm.

Fig. 2 Close-up views of various structures from cyanobacterial cell HDC images. (**a**) Schematics indicating which portions are provided in greater detail. Portion numbers

correspond to the labeled number in the first one of four figures, respectively shown in Figs. (**b**-**e**). (**b**) Thylakoid-like ultrastructural images. (**c**) Rubisco-like ultrastructural images. (**d**) Polyribosome-like ultrastructural images. (**e**) Phycobilisome-like ultrastructural images. Scale bars in (**a**), 500 nm and (**b-e**), 100 nm.

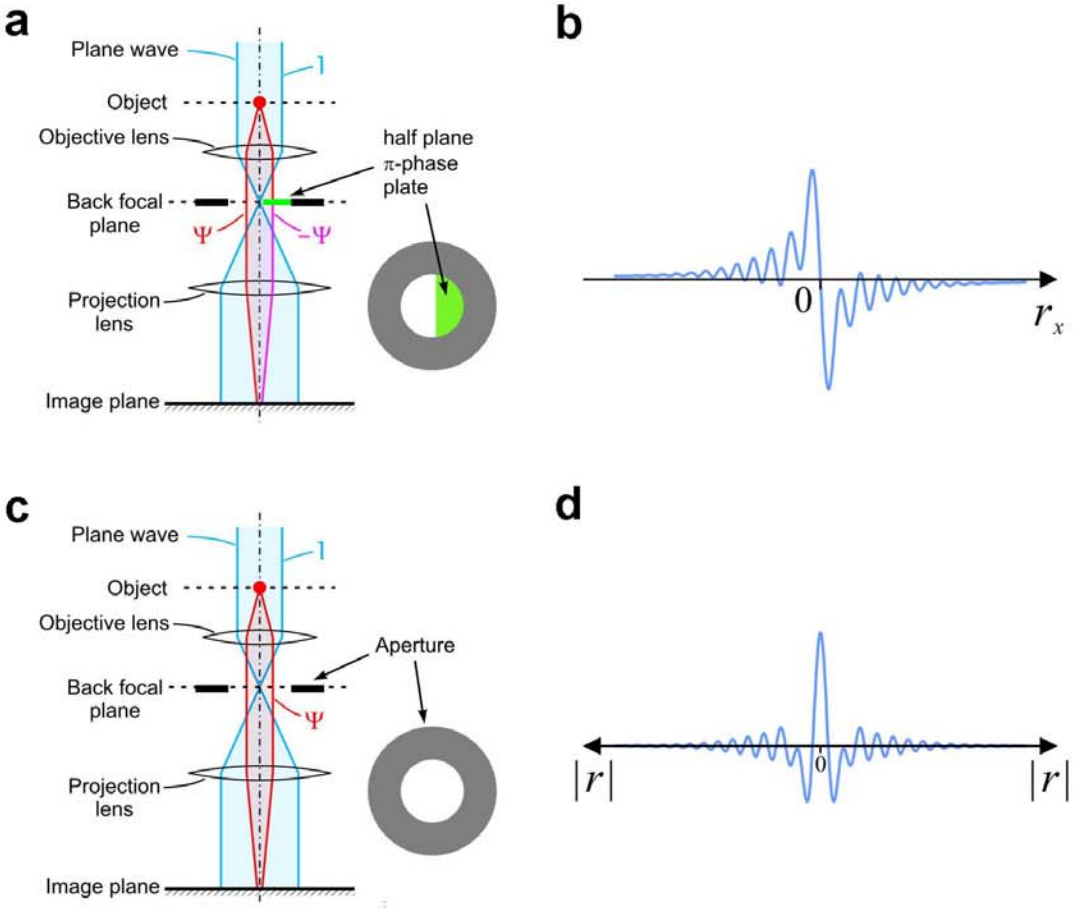
a
Plane wave
1
Object
Objective lens
half plane
π-phase
plate
Back focal
plane
Ψ
-Ψ
Projection
lens
Image plane
b
0
r_x
c
Plane wave
1
Object
Objective lens
Aperture
Back focal
plane
Ψ
Projection
lens
Image plane
d
$|r|$
0
$|r|$

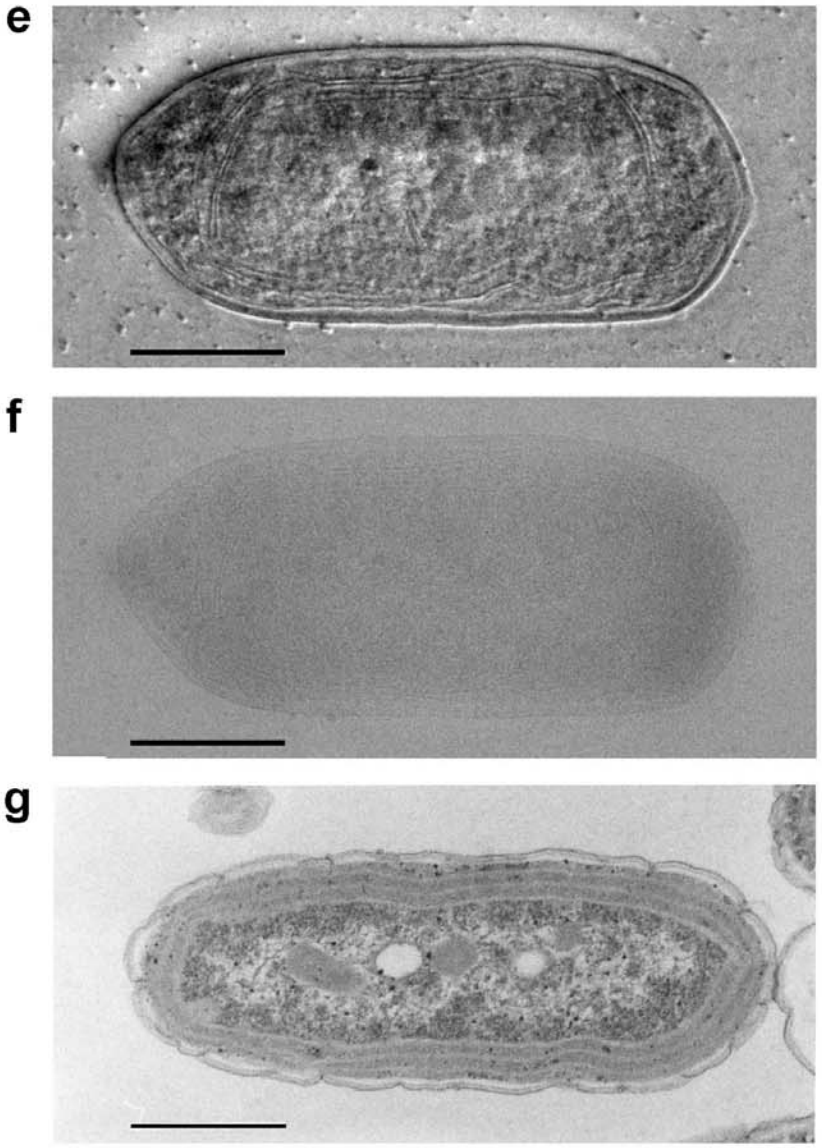
e
f
g

Figure 1

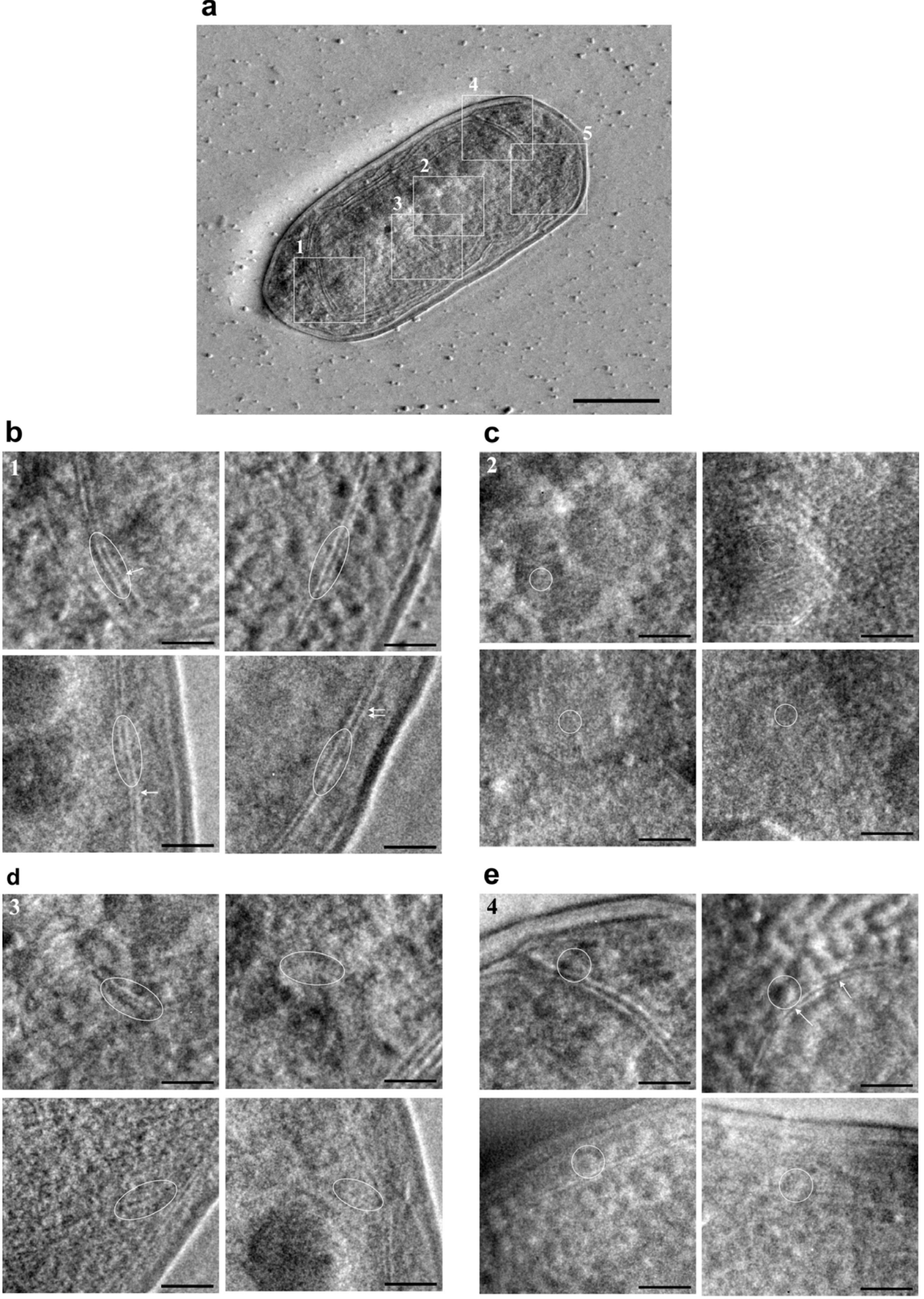

Figure 2